A GPU-Accelerated Machine Learning Framework for Molecular Simulation: Hoomd-blue with TensorFlow

Rainier Barrett[1], Maghesree Chakraborty[1], Dilnoza B. Amirkulova[1], Heta A. Gandhi[1], and Andrew D. White[1*]

[1]Department of Chemical Engineering, University of Rochester, Rochester, NY 14627

Abstract

We have designed and implemented software that enables integration of a scalable GPU-accelerated molecular mechanics engine, HOOMD-blue, with the machine learning (ML) TensorFlow package. TensorFlow is a GPU-accelerated, scalable, graph-based tensor computation model building package that has been the implementation of many recent innovations in deep learning and other ML tasks. Tensor computation graphs allow for designation of robust, flexible, and easily replicated computational models for a variety of tasks. Our plugin leverages the generality and speed of computational tensor graphs in TensorFlow to enable four previously challenging tasks in molecular dynamics: (1) the calculation of arbitrary force-fields including neural-network-based, stochastic, and/or automatically-generated force-fields which are differentiated from potential functions; (2) the efficient computation of arbitrary collective variables; (3) the biasing of simulations via automatic differentiation of collective variables and consequently the implementation of many free energy biasing methods; (4) ML on any of the above tasks, including coarse grain force fields, on-the-fly learned biases, and collective variable calculations. The TensorFlow models are constructed in Python and can be visualized or debugged using the rich set of tools implemented in the TensorFlow package. In this article, we present examples of the four major tasks this method can accomplish, and describe the architecture of our implementation. This method should lead to both the design of new models in computational chemistry research and reproducible model specification without requiring recompiling or writing low-level code.

1 Introduction

HOOMD-blue[1,2] is a GPU-accelerated engine for molecular dynamics (MD) and hard particle Monte Carlo simulations, and has simulated clathrate crystal colloids,[3] coarse grained solar cell polymers,[4] intrinsically disordered proteins,[5] and various other systems.[6–24] HOOMD-blue can simulate large systems with high speed due to the scalable nature of GPU processing. Another advantage of HOOMD-blue is that it has a Python interface that can be readily incorporated into a larger Python workflow.

TensorFlow[25] is a ML library created and maintained by Google. TensorFlow uses a graph-based computation framework with tensor operations to represent its underlying mathematical operations. This tensor graph abstraction allows for flexible model design, where one can easily add, remove, or alter operations (nodes) of a model (graph) while preserving the overall structure and flow of the tensor data (edges). TensorFlow has a built-in visualization tool called TensorBoard[25] to aid in this process. One consequence of this tensor computation graph model designation is a major advantage of TensorFlow: most of the tensor operations defined in its library are analytically differentiable, and these derivatives can be automatically propagated throughout any TensorFlow model upon request. Thus, as long as we can express a model as a composition of tensor operations, we automatically have access to its derivatives at every step to compute forces or perform learning. Additionally, TensorFlow can optimize model evaluation by caching values of tensors as they are evaluated so that branches in the graph need not have these values explicitly stored in memory.

The HTF package described in this work gives TensorFlow access to the per-particle positions, neighbor lists, and forces generated by HOOMD-blue at each time step of a simulation. Since both HOOMD-blue and TensorFlow can execute entirely on the GPU, there is minimal loss of speed due to communication. With HTF, a user may specify any tensor operation on the neighbor list and automatically calculate its derivatives and thus, its forces. This enables use of arbitrary force fields (e.g., from neural networks), calculation of arbitrary collective variables, and biasing of arbitrary collective variables. In addition, since TensorFlow contains a suite of ML algorithm implementations, a user can also perform learning on any of the items calculated using HTF.

ML has been defined a number of different ways in the past,[26–28] but for the purpose of this work, it is taken to mean a computer "learning" how to best perform some task under a given performance metric via optimization of a set of vector operations. For example, common ML applications are regression problems and classification problems, where the performance metric is usually obvious – e.g. how many items the program correctly sorts in a classification problem, or the mean squared error from a target function or distribution in a regression problem. Specifying the correct performance metric and model structure to accomplish a given task is neither deterministic nor necessarily simple,[29,30] but TensorFlow eases the process with its library of ML algorithms.

Recently, ML methods have been used to improve the accuracy of MD simulations, and some have even achieved configurational accuracy on par with ab-initio methods.[31–33] However, the way this process is typically performed can be difficult or cumbersome to reproduce.[34] This is because implementing a given ML model often requires custom low-level code to achieve learning in the context of MD simulation engines, or because it necessitates an iterative process of generating data, training, and validating, rather than a single ongoing process.[35,36] HTF can bridge this gap and make the process of connecting ML models with MD simulations easy, transparent, and reproducible via the model specification interface of TensorFlow.

The rest of this paper is broken up into five sections plus some concluding remarks. The first section summarizes the architecture of the HTF package and how it works. The remaining four sections each describe an application of HTF to a particular task in molecular dynamics, demonstrating online ML in MD, arbitrary collective variable calculations, a use-case of TensorFlow's automatic differentiation, and learning of coarse-grain forces.

2 Methods and Implementation

A more complete description of TensorFlow may be found in **(author?)**[25] TensorFlow models are built and run in separate steps, similar to how a computer program is compiled and then executed. The models in TensorFlow are expressed as tensor computation graphs where nodes are tensor operations and edges are tensors. The HTF plugin follows the same approach, whereby there is a graph building step and then an execution step. In reality, both of these steps may be performed in a single Python script. We make this conceptual distinction here for ease of discussion.

During the graph building step, placeholder tensors are accessible for neighbor lists, positions, and forces. During the execution step (i.e., running the simulation), they will be populated with their respective values in HOOMD-blue at the current time step. The native HOOMD-blue neighbor list is used. A neighbor list is an $N \times M \times 4$ tensor, where N is the number of particles, M is a pre-set maximum number of neighbors, and the last dimension is x, y, z, w. Here, w_m denotes the m^{th} neighbor's particle type, and $x_{n,m}, y_{n,m}, z_{n,m}$ are the components of the distance vector to the m^{th} neighbor of the n^{th} particle. The positions, neighbor lists, and forces are provided as possible inputs at each step. However, the format of the neighbor list is changed to a tensor to facilitate further tensor operations in HTF. Additionally, the neighbor list tensor is zero-padded to handle cases where the number of neighbors for a particle is fewer than M. Unfortunately, the optimal choice of M is not well-defined and instead must be considered on a case-by-case basis, based on available computational resources, system size, and ML model complexity. It should be noted that in HOOMD-blue the neighbor list order is not deterministic, resulting in a randomly-ordered neighbor list for each particle at each step.[1,2] In principle, learning functions that depend only on pairwise particle distance will not be affected by neighbor list order, but for cases where a sorted neighbor list is desired for specific ML objectives, HTF includes a method for enforcing ordered neighbor lists instead. For an example of a deep ML method using neighbor lists in sorted order, see **(author?)**[31]

The tensor computation graph can also output forces and a virial at each step. During the graph building step, these may be computed in the tensor computation graph or automatically calculated from a per-particle or total potential energy tensor. The neighbor lists are taken directly from HOOMD-blue and are not reconstructed. The automatic differentiation computes the forces on particles as:

$$\vec{F}_i = -\frac{\partial U(\mathbf{r})}{\partial \vec{r}_i} - \sum_{i<j} \frac{\partial U(\mathbf{r})}{\partial \vec{r}_{ij}} \tag{1}$$

where $U(\mathbf{r})$ is the potential energy as a function of both positions and/or pairwise distances, $\vec{F}_i$ is the net force on particle i, and $\vec{r}_{ij}$ is the distance vector from particle i to j. HTF computes the per-particle virial contribution from pairwise interactions only:

$$\tau_i = \sum_{i<j} \frac{F_{ij}}{r_{ij}} \left(\vec{r}_{ij} \otimes \vec{r}_{ij}\right) \tag{2}$$

Here τ_i is the virial stress tensor of particle i, F_{ij} is the magnitude of the force on particle i from particle j, and $\otimes$ indicates an outer product. If a biasing force in HTF is not pairwise additive, then the virial contribution can be computed by the user to override this default contribution.

During the execution step, while the simulation is running, the TensorFlow graph is executed with the current neighbor lists, positions and forces. Forces can be an input or output. If the TensorFlow graph outputs forces, those will be set in HOOMD-blue to be forces on the particles. Sometimes there is no output, for example if computing a collective variable. Variables in the tensor computation graph allow values to be saved and updated at each step. This allows computed quantities at all stages of the graph to be output. Further, this allows accumulation of values and thus computing quantities like running averages or time-dependent biases. The variables can also be checkpointed and restarted within HTF. During online training with HOOMD-blue, training input is not batched. Rather, based on a set parameter called "period," HTF updates its model parameters periodically throughout the ongoing HOOMD-blue simulation. Thus, a "batch" of data in the typical ML sense is a single instance of a neighbor list for each particle in the simulation.

Further details, including software architecture and benchmarking information, can be found in the supporting information.

3 Case Studies with HTF

3.1 Neural Network Force Field (Arbitrary Force Fields)

Neural networks are a powerful class of ML tools whose original theory dates back to the 1950s and 60s.[37–39] These highly flexible tools have been applied to a variety of diverse tasks in the past, including guiding surveillance technology,[40,41] tracking visual targets,[42–44] predicting cancer occurrence in patients,[45,46] processing medical imaging for enhanced diagnostic accuracy,[47] controlling the beam of a particle accelerator,[48] and aiding in finance applications.[49] They have seen recent use in molecular dynamics simulations, allowing for trained force fields that accurately reproduce experimental conformations[32] and dynamical properties in coarse-grained simulations.[31] Other recent examples include an energy-conserving force field by **(author?)**[50], later improved to include physical symmetries of molecules,[51] a multi-neural-network-based force field with DFT-level accuracy,[52] and another neural network force field based on atomic symmetry functions.[53]

The HTF plugin allows users to designate the structure of neural networks and achieve online training based on HOOMD-blue data during the HOOMD-blue simulation. Any collective variable that can be expressed as a tensor operation on the HOOMD-blue neighbor list or per-particle positions or forces can be used as training data or neural network input. As a proof of concept, we have trained a neural network to reproduce the Lennard-Jones forces on a 2D simulation of 10000 particles. Training was done online, i.e. during the simulation. The neural network input was the HOOMD-blue neighbor list, and it was trained to output the forces on each particle with an $l2$ loss function (mean squared error) and the TensorFlow built-in ADAM optimizer[54] with a learning rate $\eta = 0.001$, and with TensorFlow's default parameters of $\beta_1 = 0.9$, $\beta_2 = 0.999$, and $\epsilon = 1 \times 10^{-8}$. We employed random dropout at a rate of 20% to avoid overfitting.[55] The simulation used reduced LJ units with a time step of 0.005, and Langevin integration with $kT = 1.0$. The simulation box was created in HOOMD-blue as a square lattice with lattice constant $a = 2.0$ (100×100 2D box). A complete list of simulation and ML parameters can be found in Table 1.

The model structure was a dense neural network with three layers: one input layer, one hidden layer, and one output layer. Each layer is size 20 and uses a tanh activation function, except the output layer, which had no activation function. A neural network can be thought of as repeated application of operations $\{\mathcal{F}_i\}$ defined in eq 3, where $\vec{w}_i$ is a weight vector and $\vec{b}_i$ is a bias vector, both of which are unique to each layer, and $\vec{x}_i$ is the vector of input values to layer i. σ_i is some activation function. The limiting case of an activation function is a linear activation, which is the same as "no activation", where $\sigma(x) = x$. This is rarely used, however, since only neural networks with non-linear activation functions can serve as universal function

Simulation Parameters (LJ reduced units)	
Dimension	2D
Ensemble	NVT
Thermostat	Langevin
Box Size	100
time step	0.005
kT	1.0
Force Field	Lennard-Jones
Cutoff Radius	3.0
$N_{\text{particles}}$	10000
Langevin γ	1.0
Lennard-Jones Parameters	
ϵ	1.0
σ	1.0
Neural Network Hyperparameters	
N_{hidden}	1
Nodes per Layer	20
Activation Function	tanh
Optimizer	Adam[54]
Dropout Rate	0.2
Adam Parameters	
Learning Rate	0.005
β_1	0.9
β_2	0.999
ϵ	10^{-8}
HTF Parameters	
Period	10
M	63

Table 1 NN Force Field Simulation Parameters.

approximators.[56] Common activation functions include the sigmoid, $\sigma(x) = \frac{1}{1+e^{-x}}$, $\tanh(x)$, and relu ("rectified linear unit"), $\sigma(x) = \max(0, x)$.

$$\mathcal{F}_i\left(\vec{x}_i\right) = \sigma_i(\vec{w}_i \cdot \vec{x}_i + \vec{b}_i) \tag{3}$$

In this case, the neural network's output is then $\mathcal{F}_2\left(\mathcal{F}_1\left(\mathcal{F}_0\left(\vec{x}\right)\right)\right)$, with $\sigma_0(x) = \sigma_1(x) = \tanh(x)$ and $\sigma_2(x) = x$. The final layer uses a linear activation function to allow for values of greater magnitude than 1.0. The trained quantities are the weight and bias vectors. The input is $\vec{x} = \vec{r}^{-1}$, the vector of inverse distances between each particle and the particles in its neighbor list.

After a 4000 step equilibration period, the model was trained for 500000 steps, which can be done in minutes using a GPU-enabled compute node (NVIDIA Tesla V100). The $l2$ loss of the model over time is shown in Figure 1. The model converged after 450000 time steps with a final loss value of 0.25.

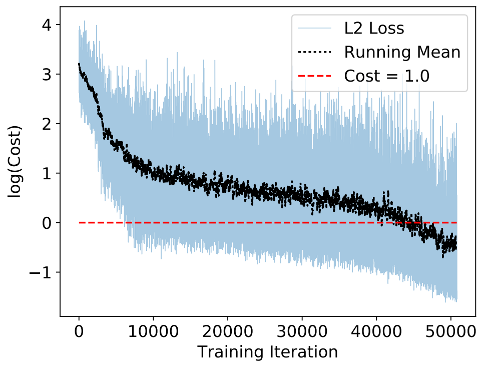

(a)

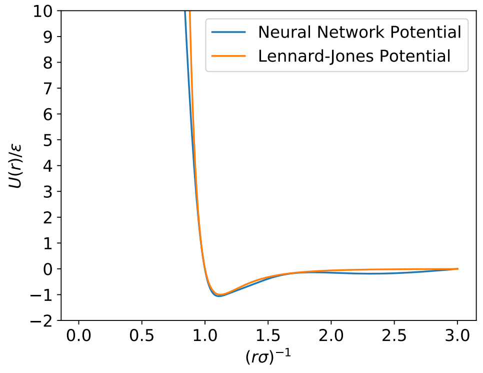

(b)

Figure 1 Using a simple neural network in a 10000 particle Lennard-Jones simulation to learn the Lennard-Jones force field. **(a):** The $l2$ loss over time of the neural network force field during training (log scale). The $l2$ loss is computed as the mean squared difference between the Lennard-Jones forces calculated by HOOMD-blue and those generated by the neural network. The dashed red line shows when cost falls below 1.0, an arbitrary signifier of "good agreement." **(b):** Comparison of the learned potential and the true Lennard-Jones potential, showing recovery of the key features of the Lennard-Jones force field.

3.2 Force Matching (Learning)

Bottom-up coarse graining (CG)[57–59] has been used to model various systems like alkanes[59], polymers[60], and biomolecules.[57] In the bottom-up approach, the CG potentials are derived from the underlying all-atom (AA) simulation. Force-matching (FM)[61–63] is a bottom-up CG approach which aims to match the forces on CG particles as closely as possible to the cumulative forces on their constituent atoms in the reference AA simulation.[57] Besides obtaining the CG potential, another vital step in defining the CG system is to determine the mapping operator, which indicates how atoms in the AA system are grouped into CG particles. The general practice to define a CG mapping operator has historically been driven by chemical intuition.[64] However, recently there have been efforts toward choosing mapping operators more systemically.[65–67]

In the following section, let $\mathbf{r}$ represent the coordinates of particles in an all-atom simulation, and let $\mathbf{R}$ represent the corresponding coarse-grained particle positions. The reference mapped force is calculated by eq 4, where F_I^{ref} is the force on the I^{th} CG particle, S_I refers to the subset of particles which are mapped into the I^{th} CG particle and $\vec{F_i}$ is the net force on the i^{th} particle in the AA model.

$$\mathbf{F}_I^{ref}(\mathbf{r}) = \sum_{i \in S_I} \vec{F_i}(\mathbf{r}) \tag{4}$$

The FM method finds $\mathbf{F}^{CG}(\mathbf{R})$ that minimizes the objective function given by eq 5,

$$\chi^2 = \left\langle \frac{1}{3N} \sum_{I=1}^{N} \left| \mathbf{F}_I^{CG}(\mathbf{R}) - \mathbf{F}_I^{ref}(\mathbf{r}) \right|^2 \right\rangle \tag{5}$$

where N is the number of CG particles and the angular brackets denote an ensemble average. In the most common implementation, $\mathbf{F}^{CG}(\mathbf{R})$ is approximated using cubic splines as the basis set.[62,68]

Previous studies have reported the use of various ML techniques for CG models.[31,69] Here we model the CG potential using a basis set ($\mathcal{B}$) of 48 Gaussian functions and a repulsive term, $U_{rep}(R) = u(R - r_0)(R - r_0)^{12}$, where $u()$ is the unit step function, R is the pairwise distance between particles, and r_0 is a fitting parameter. The variance and the height of each of the Gaussian functions in the basis set were trained on-the-fly using mapped CG positions from an atomistic simulation of methanol molecules in HOOMD-blue using the parameters given in Table 2. Each methanol molecule was mapped to one CG bead at its center of mass (COM). Corresponding mapped pairwise distances were calculated considering 128 nearest neighbors.

The optimization was done at a learning rate of 0.1 using the ADAM optimizer[54] by minimizing the objective function given by eq 6

$$\chi^2 = \left\langle \frac{1}{3N} \sum_{I=1}^{N} \left| \mathbf{F}_I^{\mathcal{B}}(\mathbf{R}) - \mathbf{F}_I^{ref}(\mathbf{r}) \right|^2 \right\rangle - r_0 \tag{6}$$

where $\mathbf{F}_I^{\mathcal{B}}$ refers to the forces calculated using the basis set and the mapped pairwise distances and r_0 is a fitting parameter for the repulsive function U_{rep}. In eq 6, the first term is the mean squared error between the mapped CG forces from the atomistic simulation and the forces calculated using the the basis set, and the last term pushes the short range repulsive term to the right. A cutoff radius of 12 Å was used for the simulation. After equilibrating

Dimension	3D
Ensemble	NVT
Thermostat	Nosé-Hoover
Density	778 kg/m^3
time step	2 fs
Temperature	300 K
Force Field	OPLS-AA
Cutoff Radius	10
$N_{\text{molecules}}$	256

Table 2 Simulation Parameters for AA Methanol.

the CG system, the production CG simulation was run for 10,000 time steps. Figure 2 shows the learned CG potential along with the locations of the Gaussian basis set functions of $\mathcal{B}$. The locations of the minima in the learned CG potential conform well with those reported in previous studies[70–72] which used conventional tools for FM. Figure 3 compares the COM radial distribution function (RDF) obtained from the AA simulation and that obtained from running a CG simulation using the learned potentials. The RDF shows good agreement.

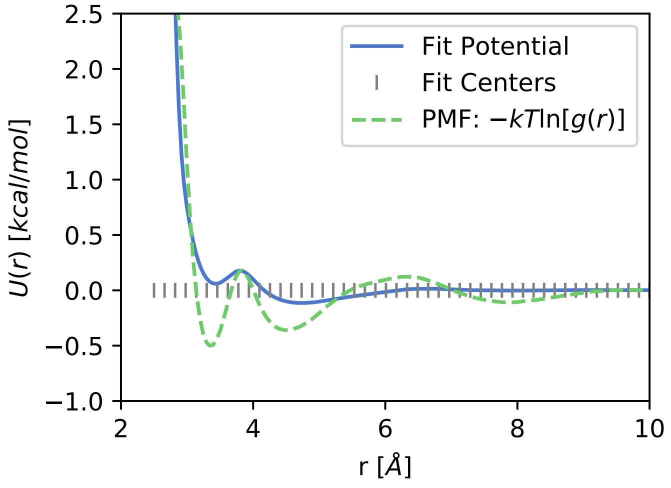

Figure 2 The learned CG potential along with the fit centers of the Gaussian basis set functions for a one bead methanol simulation. A reference potential of mean force (PMF) computed as $-kT\ln[g(r)]$ is plotted. Agreement between CG potential and PMF is not expected, but provides a reference for location of potential energy minima. The repulsion term provides stronger repulsion than is possible with the Gaussian basis set alone.

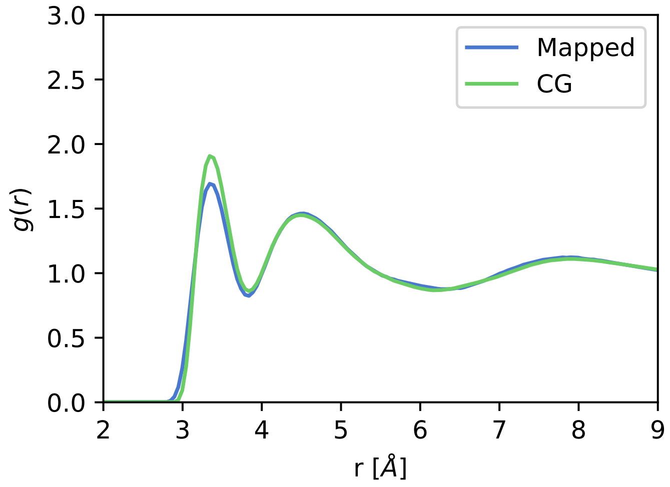

Figure 3 The center of mass radial distribution function from the AA (Mapped) and the CG simulation of methanol. The one bead CG simulation shows good agreement with a mapped AA simulation.

3.3 EDS in HTF (Biasing/Automatic differentiation)

Simulations often do not agree with experiments or quantum mechanics results due to force-field or time-scale limitations.[73] However, simulations can be biased to agree with experimental observables or reference values.[74] Experiment Directed Simulation (EDS) is a maximum-entropy biasing technique used to match simulations with some experimental observables.[74] EDS minimally modifies the free energy surface of a simulation such that average values of simulated collective variables (CVs) match specified average reference values.[74] If instead of a single average value, an entire free energy distribution along a CV needs to match a target free energy distribution, Experiment Directed Metadynamics can be applied.[75] EDS can match multiple experimental values in a single iteration of the simulation.[74] EDS has been previously applied in various systems such as Li ion battery and bead-spring polymer models,[74] a water model,[76] a peptide model,[73] and in coarse graining techniques.[77] Dynamical studies of water with EDS showed improved prediction of both biased and unbiased dynamic properties, which are known to be hard to reproduce even with quantum mechanics.[76] This is possible because EDS minimally modifies the free energy surface and allows accurate prediction of dynamical and structural properties. A recent review on EDS and other maximum entropy methods can be found in Amirkulova and White.[78] In this work EDS was implemented in the TensorFlow framework in HTF.

In EDS, the potential energy, $U(\vec{r})$ is modified minimally with addition of multiple coupling constants, α_j, as shown in eq 7, where the index j is over the number of CVs to be biased. We desire that the ensemble average of a simulated CV, $f(\vec{r})$, satisfy $\langle f(\vec{r})\rangle = \hat{f}$, where $\langle f(\vec{r})\rangle$ is the ensemble average of the CV and $\hat{f}$ is the reference value of that CV. The force of the i^{th} particle, is calculated from the potential given by eq 7 at each time step.

$$U'(\vec{r}, \alpha) = U(\vec{r}) + \sum_j \alpha_j \frac{f_j(\vec{r})}{\bar{f}_j} \tag{7}$$

Simulation Parameters	
Dimension	2D
Ensemble	NVT
Thermostat	Langevin
Box Size	16×16
time step	0.005
kT	1.0
Velocity Randomization Seed	40
Force Field	Lennard-Jones
Cutoff Radius	3.0
$N_{\text{particles}}$	64
Langevin γ	1.0
Lennard-Jones Parameters	
ϵ	1.0 (reduced units)
σ	1.0 (reduced units)
HTF Parameters	
Period	10
M	63
EDS Parameters	
Period	20
Range	0.3
Save Period	1000
$\bar{f}$	5.8

Table 3 EDS Simulation Parameters.

$$\hat{R}_{COM} = \frac{1}{N}\sum_{i}^{N} |\vec{r}_i - \vec{r}_{COM}| \tag{8}$$

A Lennard-Jones particle simulation was performed, and biased with EDS. Mean radius ($\hat{R}_{COM}$), which is defined in eq 8, is an average of absolute differences between each particle position and the center of mass (COM) of all N particles. By using the mean radius as a CV for EDS, we can enforce the simulation on average to form a circle around the COM with a radius of a reference value. We ran EDS and control simulations of Lennard-Jones particles in the canonical ensemble with parameters shown in table 3. We assigned random initial velocities to the particles. The only difference between the EDS and control simulations was biasing the potential energy of the EDS simulation at every HTF iteration, which corresponds to "Period" in the EDS Parameters section of table 3. The "Range" parameter indicates the range of coupling constant values for the EDS bias, in reduced energy units.

We biased the EDS simulation such that the ensemble average of $\hat{R}_{COM}$ matches a reference value of 5.8, as shown in fig 4. In fig 4, the average $\hat{R}_{COM}$ in the EDS simulation, shown in green, oscillates and finally matches the reference value, shown in red. In comparison, the control simulation has an average $\hat{R}_{COM}$ of 6.1. The distribution of particle positions in the simulation box is shown as a heatmap averaged over all all time steps in fig 5. EDS tries to force the particles to form a circle around the center of the box, but this is not energetically

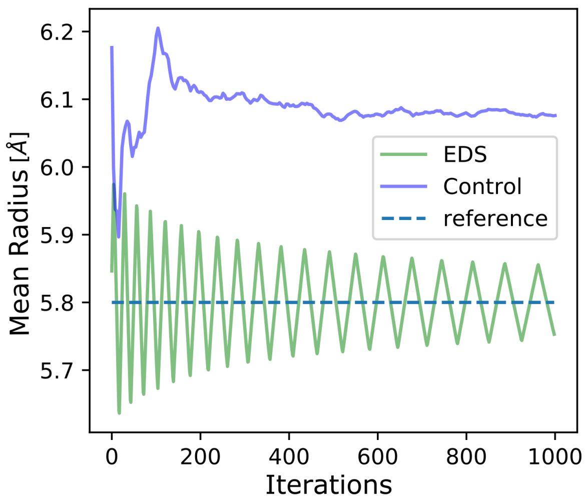

Figure 4 EDS matches a reference set-point value with addition of bias. At the end of the EDS simulation, the average radius agrees with the reference value of 5.8. The control simulation converges to an average radius around 6.1 and does not converge to the reference value. Each iteration consists of 6000 time steps.

favorable due to repulsion effects. Instead, as seen in in fig 5 (A), particles are mostly inside or outside of the circle of radius 5.8. Although these particles are either on the inside or the outside of this circle, they are distributed in such a way that their average $\hat{R}_{COM}$ is 5.8, due to the EDS bias. The particles in the control simulation are distributed more uniformly as shown in fig 5 (B), where all positions are roughly equally likely.

We have shown that EDS can modify a simulation such that there is an agreement between simulations and chosen observables. This technique can be applied to larger and more complex systems in HOOMD-blue where there may exist a major discrepancy between simulations and experiments.

3.4 Calculating Scattering Profiles (Arbitrary Collective Variables)

Scattering techniques are used extensively for material characterization and structure determination.[79] Neutron scattering in particular has applications in the field of condensed matter physics,[80,81] nuclear physics and nuclear materials research,[82] biology,[83] crystallography, and catalysis.[81] For this work, we demonstrate that HTF can be used to approximate the neutron scattering profile of a simulation box at every time step, on-the-fly.

The neutron scattering profile for particles can be analytically estimated using Debye's formula given by eq (9).[84]

$$I(q) = \sum_i \sum_j b_i b_j \frac{\sin(q\ r_{ij})}{q\ r_{ij}} \tag{9}$$

Here, b_i and b_j are the coherent scattering lengths for the particles i and j respectively, r_{ij} is the inter-particle distance between particles i and j, and q is the magnitude of $\vec{q}$, the scattering vector or the momentum transfer vector, which is a function of the scattering angle θ and

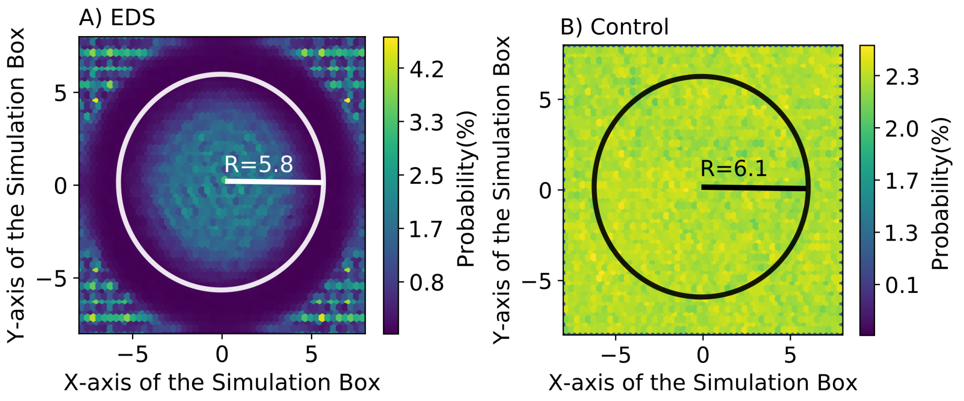

Figure 5 Lennard Jones particles are biased to reside inside the circle during EDS. EDS (A) allows particles to be inside of a circle with a radius of 5.8. Control (B) particles do not form a circle with mean radius of 6.1, which was the average radius computed during the control simulation. The circles with radii corresponding to the average radii of particles away from the COM are shown in white. The average radius of 5.8 during EDS (A) agrees with the reference value of 5.8, as opposed to value of 6.1 (B).

wavelength λ. The data for scattering lengths of different particles is available in literature.[85]

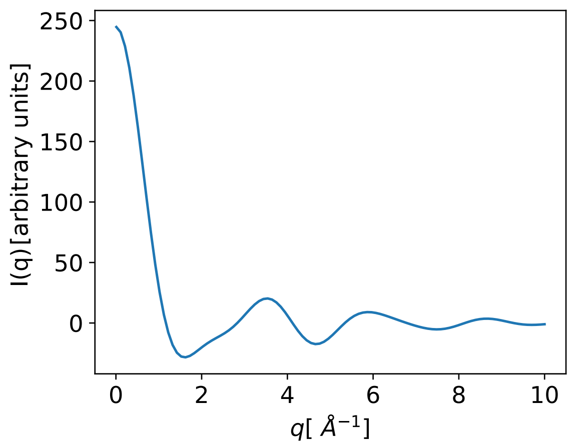

Figure 6 The neutron scattering profile for 5000 H_2O molecules calculated using HTF. Scattering intensities are calculated for every value of q at each time step on-the-fly and the averaged intensities over all time steps are presented here.

A box of 5000 water molecules was simulated in order to calculate their neutron scattering profile. Figure 6 shows the resultant scattering profile, which was calculated as an average of the scattering intensities at each time step during the simulation. The simulation details are given in Table 4. The obtained scattering profile (Figure 6) is in close agreement with the experimentally observed neutron scattering profile for H_2O from **(author?)**[86]

Due to the automatic differentiation included in TensorFlow, a more complex system could be conveniently biased toward an experimentally obtained neutron scattering profile on-the-fly, without necessitating tracking the analytic derivative of eq 9 with respect to r_{ij} of every pair of particles for every value of q.

Simulation Parameters (LJ reduced units)	
Dimension	3D
Ensemble	NVT
Thermostat	Nosé-Hoover
Box Size	53.1
time step	0.04
Total time steps	0.04
T	298 K
Force Field	OPLS-AA
Water Model	TIP3P
Cutoff Radius	4.0
$N_{\text{molecules}}$	5000
Nosé-Hoover τ	2.0
Neutron Scattering Lengths	
b_H	-3.742
b_O	5.805
HTF Parameters	
Period	10
M	256

Table 4 H_2O Simulation Parameters to Calculate Scattering Profile.

4 Concluding Remarks

We have presented a general tool for utilizing TensorFlow in the MD and MC simulation engine HOOMD-blue. TensorFlow's tensor computation graphs are expressive enough to allow force-fields, biasing methods, learning, and collective variable computation within a single framework. HTF enables GPU-accelerated and low-latency use of TensorFlow in HOOMD-blue and thus makes online learning in a simulation possible with little additional effort. The online nature of learning in HTF simplifies the "traditional" workflow of ML in simulations by removing the need for post-processing of trajectories or custom implementations of common ML algorithms. The tensor computation graphs allow for transparent and simple model designation with a high degree of customizability, replicability, and efficiency.

The HTF source code is available as specified in the Supporting Information where each of the systems presented in this article are available as examples.

5 Acknowledgements

The authors would like to thank Joshua Anderson and Jens Glaser for instructive conversations about the HOOMD-blue architecture. The authors thank the Center for Integrated Research Computing (CIRC) at the University of Rochester for providing computational resources and technical support. This work was supported by the National Science Foundation (CBET-1751471 and CHE-1764415).

References

1. Joshua A. Anderson, Chris D. Lorenz, and A. Travesset. General purpose molecular dynamics simulations fully implemented on graphics processing units. *J. Comput. Phys.*, 227(10):5342–5359, may 2008.

2. Jens Glaser, Trung Dac Nguyen, Joshua A. Anderson, Pak Lui, Filippo Spiga, Jaime A. Millan, David C. Morse, and Sharon C. Glotzer. Strong scaling of general-purpose molecular dynamics simulations on GPUs. *Comput. Phys. Commun.*, 192:97–107, jul 2015.

3. Haixin Lin, Sangmin Lee, Lin Sun, Matthew Spellings, Michael Engel, Sharon C Glotzer, and Chad A Mirkin. Clathrate colloidal crystals. *Science*, 355(6328):931–935, mar 2017.

4. Nanjia Zhou, Alexander S Dudnik, Ting I N G Li, Eric F Manley, Thomas J Aldrich, Peijun Guo, Hsueh-Chung Liao, Zhihua Chen, Lin X Chen, Robert P H Chang, Antonio Facchetti, Monica Olvera De La Cruz, and Tobin J Marks. All-Polymer Solar Cell Performance Optimized via Systematic Molecular Weight Tuning of Both Donor and Acceptor Polymers. *J. Am. Chem. Soc.*, 138(4):1240–1251, 2015.

5. Gregory L Dignon, Wenwei Zheng, Robert B Best, Young C Kim, and Jeetain Mittal. Relation between single-molecule properties and phase behavior of intrinsically disordered proteins. *Proc. Natl. Acad. Sci. U. S. A.*, 115(40):9929–9934, oct 2018.

6. Rodrigo E. Guerra, Colm P. Kelleher, Andrew D. Hollingsworth, and Paul M. Chaikin. Freezing on a sphere. *Nature*, 554(7692):346–350, feb 2018.

7. Emmanuel Millán Kujtiuk, Eduardo M Bringa, Andrew Higginbotham, and Carlos Garcia Garino. GP-GPU Processing of Molecular Dynamics Simulations. In *HPC - LATAM*, pages 3234–3248, Buenos Aires, 2010.

8. Lin Yang, Feng Zhang, Cai-Zhuang Wang, Kai-Ming Ho, and Alex Travesset. Implementation of metal-friendly EAM/FS-type semi-empirical potentials in HOOMD-blue: A GPU-accelerated molecular dynamics software. *J. Comput. Phys.*, 359:352–360, apr 2018.

9. Trung Dac Nguyen, Carolyn L. Phillips, Joshua A. Anderson, and Sharon C. Glotzer. Rigid body constraints realized in massively-parallel molecular dynamics on graphics processing units. *Comput. Phys. Commun.*, 182(11):2307–2313, nov 2011.

10. Andrew W. Long, Carolyn L. Phillips, Eric Jankowski, and Andrew L. Ferguson. Nonlinear machine learning and design of reconfigurable digital colloids. *Soft Matter*, 12(34):7119–7135, aug 2016.

11. David N. LeBard, Benjamin G. Levine, Russell DeVane, Wataru Shinoda, and Michael L. Klein. Premicelles and monomer exchange in aqueous surfactant solutions above and below the critical micelle concentration. *Chem. Phys. Lett.*, 522:38–42, jan 2012.

12. I.V. Morozov, A.M. Kazennov, R.G. Bystryi, G.E. Norman, V.V. Pisarev, and V.V. Stegailov. Molecular dynamics simulations of the relaxation processes in the condensed matter on GPUs. *Comput. Phys. Commun.*, 182(9):1974–1978, sep 2011.

13. Lisa Teich and Christian Schroder. Numerical Investigation of the Magnetodynamics of Self-Organizing Nanoparticle Ensembles: A Hybrid Molecular and Spin Dynamics Approach. *IEEE Trans. Magn.*, 51(11):1–4, nov 2015.

14. Caleb L. Breaux, Jakin B. Delony, Peter J. Ludovice, and Clifford L. Henderson. Effect of homopolymer concentration on LER and LWR in block copolymer/homopolymer blends. In Eric M. Panning and Martha I. Sanchez, editors, *Nov. Patterning Technol. 2018*, volume 10584, page 52. SPIE, apr 2018.

15. Fabrizio Benedetti, Dusan Racko, Julien Dorier, Yannis Burnier, and Andrzej Stasiak. Transcription-induced supercoiling explains formation of self-interacting chromatin domains in S. pombe. *Nucleic Acids Res.*, 45(17):9850–9859, sep 2017.

16. Fabrizio Benedetti, Aleksandre Japaridze, Julien Dorier, Dusan Racko, Robert Kwapich, Yannis Burnier, Giovanni Dietler, and Andrzej Stasiak. Effects of physiological self-crowding of DNA on shape and biological properties of DNA molecules with various levels of supercoiling. *Nucleic Acids Res.*, 43(4):2390–2399, feb 2015.

17. Carolyn L. Phillips, Joshua A. Anderson, and Sharon C. Glotzer. Molecular Dynamics Models of Shaped Particles Using Filling Solutions. *Phys. Procedia*, 53:75–81, jan 2014.

18. Benjamin Trefz and Peter Virnau. Scaling behavior of topologically constrained polymer rings in a melt. *J. Phys. Condens. Matter*, 27(35):354110, sep 2015.

19. Michael P. Howard, Athanassios Z. Panagiotopoulos, and Arash Nikoubashman. Efficient mesoscale hydrodynamics: Multiparticle collision dynamics with massively parallel GPU acceleration. *Comput. Phys. Commun.*, 230:10–20, sep 2018.

20. Benjamin G. Levine, David N. LeBard, Russell DeVane, Wataru Shinoda, Axel Kohlmeyer, and Michael L. Klein. Micellization Studied by GPU-Accelerated Coarse-Grained Molecular Dynamics. *J. Chem. Theory Comput.*, 7(12):4135–4145, dec 2011.

21. Carolyn L. Phillips, Joshua A. Anderson, and Sharon C. Glotzer. Pseudo-random number generation for Brownian Dynamics and Dissipative Particle Dynamics simulations on GPU devices. *J. Comput. Phys.*, 230(19):7191–7201, aug 2011.

22. Michael P. Howard, Joshua A. Anderson, Arash Nikoubashman, Sharon C. Glotzer, and Athanassios Z. Panagiotopoulos. Efficient neighbor list calculation for molecular simulation of colloidal systems using graphics processing units. *Comput. Phys. Commun.*, 203:45–52, jun 2016.

23. Joshua A. Anderson, M. Eric Irrgang, and Sharon C. Glotzer. Scalable Metropolis Monte Carlo for simulation of hard shapes. *Comput. Phys. Commun.*, 204:21–30, jul 2016.

24. Matthew Spellings, Ryan L. Marson, Joshua A. Anderson, and Sharon C. Glotzer. GPU accelerated Discrete Element Method (DEM) molecular dynamics for conservative, faceted particle simulations. *J. Comput. Phys.*, 334:460–467, apr 2017.

25. Martín Abadi, Ashish˜Agarwal, Paul˜Barham, Eugene˜Brevdo, Zhifeng˜Chen, Craig˜C-itro, Greg˜S.˜Corrado, Andy˜Davis, Jeffrey˜Dean, Matthieu˜Devin, Sanjay˜Ghemawat,

Ian~Goodfellow, Andrew~Harp, Geoffrey~Irving, Michael~Isard, Yangqing Jia, Rafal~Jozefowicz, Lukasz~Kaiser, Manjunath~Kudlur, Josh~Levenberg, Dandelion~Mané, Rajat~-Monga, Sherry~Moore, Derek~Murray, Chris~Olah, Mike~Schuster, Jonathon~Shlens, Benoit~Steiner, Ilya~Sutskever, Kunal~Talwar, Paul~Tucker, Vincent~Vanhoucke, Vijay~-Vasudevan, Fernanda~Viégas, Oriol~Vinyals, Pete~Warden, Martin~Wattenberg, Martin~Wicke, Yuan~Yu, and Xiaoqiang~Zheng. TensorFlow: Large-Scale Machine Learning on Heterogeneous Systems, 2015.

26. Hua Wang, Cuiqin Ma, and Lijuan Zhou. A Brief Review of Machine Learning and Its Application. In *2009 Int. Conf. Inf. Eng. Comput. Sci.*, pages 1–4. IEEE, dec 2009.

27. Kevin P. Murphy. *Machine learning : a probabilistic perspective.* MIT Press, 2012.

28. Ethem Alpaydin. *Introduction to machine learning.* MIT press, 2009.

29. Avrim L. Blum and Pat Langley. Selection of relevant features and examples in machine learning. *Artif. Intell.*, 97(1-2):245–271, dec 1997.

30. Chris. McDonald and Lloyd A. Smith. *Computer science '98 : proceedings of the 21st Australasian Computer Science Conference, ACSC'98, Perth, 4-6 February 1998*, volume Volume 20. Springer, 1998.

31. Linfeng Zhang, Jiequn Han, Han Wang, Roberto Car, and Weinan E. DeePCG: Constructing coarse-grained models via deep neural networks. *J. Chem. Phys.*, 149(3):034101, jul 2018.

32. Kun Yao, John E. Herr, David W. Toth, Ryker Mckintyre, and John Parkhill. The TensorMol-0.1 model chemistry: a neural network augmented with long-range physics. *Chem. Sci.*, 9(8):2261–2269, feb 2018.

33. Han Wang, Linfeng Zhang, Jiequn Han, and Weinan E. DeePMD-kit: A deep learning package for many-body potential energy representation and molecular dynamics. *Comput. Phys. Commun.*, 228:178–184, jul 2018.

34. Katja Hansen, Grégoire Montavon, Franziska Biegler, Siamac Fazli, Matthias Rupp, Matthias Scheffler, O. Anatole von Lilienfeld, Alexandre Tkatchenko, and Klaus-Robert Müller. Assessment and Validation of Machine Learning Methods for Predicting Molecular Atomization Energies. *J. Chem. Theory Comput.*, 9(8):3404–3419, aug 2013.

35. Matthias Rupp, Alexandre Tkatchenko, Klaus-Robert Müller, and O Anatole Von Lilienfeld. Fast and Accurate Modeling of Molecular Atomization Energies with Machine Learning. *Phys. Rev. Lett.*, 108:058301, 2012.

36. Venkatesh Botu and Rampi Ramprasad. Adaptive Machine Learning Framework to Accelerate Ab Initio Molecular Dynamics. *Int. J. Quantum Chem.*, (115):1074–1083, 2015.

37. Bernard Widrow. *Adaptive "adaline" neuron using chemical "memistors".* Stanford University, Stanford, 1960.

38. J A Anderson and E Rosenfeld. *Talking Nets: An Oral History of Neural Networks.* Bradford Books. MIT Press, 2000.

39. John Von Neumann and Others. *The general and logical theory of automata*, volume 5. New York: John Wiley& Sons, 1951.

40. T. Jan. Neural network based threat assessment for automated visual surveillance. In *2004 IEEE Int. Jt. Conf. Neural Networks (IEEE Cat. No.04CH37541)*, volume 2, pages 1309–1312. IEEE, 2004.

41. Gaige Wang, Lihong Guo, and Hong Duan. Wavelet neural network using multiple wavelet functions in target threat assessment. *ScientificWorldJournal.*, 2013:632437, feb 2013.

42. Chin-Der Wann and S.C.A. Thomopoulos. Unsupervised learning neural networks with applications to data fusion. In *Proc. 1994 Am. Control Conf. - ACC '94*, volume 2, pages 1361–1365. IEEE, 1994.

43. S. Shams. Neural network optimization for multi-target multi-sensor passive tracking. *Proc. IEEE*, 84(10):1442–1457, 1996.

44. Seunghoon Hong, Tackgeun You, Suha Kwak, and Bohyung Han. Online Tracking by Learning Discriminative Saliency Map with Convolutional Neural Network. In *32 nd Int. Conf. Mach. Learn.*, pages 1–10, 2015.

45. Murat Karabatak and M. Cevdet Ince. An expert system for detection of breast cancer based on association rules and neural network. *Expert Syst. Appl.*, 36(2):3465–3469, mar 2009.

46. Zhi-Hua Zhou, Yuan Jiang, Yu-Bin Yang, and Shi-Fu Chen. Lung cancer cell identification based on artificial neural network ensembles. *Artif. Intell. Med.*, 24(1):25–36, jan 2002.

47. A. S. Miller, B. H. Blott, and T. K. Hames. Review of neural network applications in medical imaging and signal processing. *Med. Biol. Eng. Comput.*, 30(5):449–464, sep 1992.

48. Bernard Widrow, David E. Rumelhart, and Michael A. Lehr. Neural networks: applications in industry, business and science. *Commun. ACM*, 37(3):93–106, mar 1994.

49. Bo K Wong, Thomas A Bodnovich, and Yakup Selvi. Neural network applications in business: A review and analysis of the literature (1988–1995). *Decis. Support Syst.*, 19(4):301–320, apr 1997.

50. Stefan Chmiela, Alexandre Tkatchenko, Huziel E. Sauceda, Igor Poltavsky, Kristof T. Schütt, and Klaus-Robert Müller. Machine learning of accurate energy-conserving molecular force fields. *Sci. Adv.*, 3(5):e1603015, may 2017.

51. Stefan Chmiela, Huziel E. Sauceda, Klaus-Robert Müller, and Alexandre Tkatchenko. Towards exact molecular dynamics simulations with machine-learned force fields. *Nat. Commun.*, 9(1):3887, dec 2018.

52. J. S. Smith, O. Isayev, and A. E. Roitberg. ANI-1: an extensible neural network potential with DFT accuracy at force field computational cost. *Chem. Sci.*, 8(4):3192–3203, mar 2017.

53. Yufeng Huang, Jun Kang, William A. Goddard, and Lin-Wang Wang. Density functional theory based neural network force fields from energy decompositions. *Phys. Rev. B*, 99(6):064103, feb 2019.

54. Diederik P. Kingma and Jimmy Ba. Adam: A method for stochastic optimization. *CoRR*, abs/1412.6980, 2014.

55. Nitish Srivastava, Geoffrey Hinton, Alex Krizhevsky, and Ruslan Salakhutdinov. Dropout: A Simple Way to Prevent Neural Networks from Overfitting. Technical report, 2014.

56. Moshe Leshno, Vladimir Ya. Lin, Allan Pinkus, and Shimon Schocken. Multilayer feedforward networks with a nonpolynomial activation function can approximate any function. *Neural Networks*, 6(6):861 – 867, 1993.

57. Helgi I. Ingólfsson, Cesar A. Lopez, Jaakko J. Uusitalo, Djurre H. de Jong, Srinivasa M. Gopal, Xavier Periole, and Siewert J. Marrink. The Power of Coarse Graining in Biomolecular Simulations. *Wiley Interdisciplinary Reviews: Computational Molecular Science*, 4(3):225–248, 2014.

58. Patrick G. Lafond and Sergei Izvekov. Multiscale Coarse-Graining with Effective Polarizabilities: A Fully Bottom-Up Approach. *Journal of Chemical Theory and Computation*, 14(4):1873–1886, 2018.

59. Nicholas J.H. Dunn and W. G. Noid. Bottom-up coarse-grained models that accurately describe the structure, pressure, and compressibility of molecular liquids. *Journal of Chemical Physics*, 143(24), 2015.

60. Vaidyanathan Sethuraman, Santosh Mogurampelly, and Venkat Ganesan. Multiscale Simulations of Lamellar PS-PEO Block Copolymers Doped with LiPF6 Ions. *Macromolecules*, 50(11):4542–4554, 2017.

61. F Ercolessi and J B Adams. Interatomic Potentials from First-Principles Calculations: The Force-Matching Method. *EPL (Europhysics Letters)*, 26(8):583, 1994.

62. Sergei Izvekov and Gregory A Voth. Multiscale coarse graining of liquid-state systems. *Journal of Chemical Physics*, 123(13), oct 2005.

63. Avisek Das, Lanyuan Lu, Hans C. Andersen, and Gregory A. Voth. The multiscale coarse-graining method. X. Improved algorithms for constructing coarse-grained potentials for molecular systems. *Journal of Chemical Physics*, 136(19), 2012.

64. Joseph F. Rudzinski and William G. Noid. Investigation of coarse-grained mappings via an iterative generalized Yvon-Born-Green method. *Journal of Physical Chemistry B*, 118(28):8295–8312, 2014.

65. Maghesree Chakraborty, Chenliang Xu, and Andrew D. White. Encoding and Selecting Coarse-Grain Mapping Operators with Hierarchical Graphs. *J. Chem. Phys.*, 149(13):134106, apr 2018.

66. Emiliano Brini, Elena a. Algaer, Pritam Ganguly, Chunli Li, Francisco Rodríguez-Ropero, and Nico F. a. Van Der Vegt. Systematic Coarse-Graining Methods for Soft Matter Simulations – A Review. *Soft Matter*, 9(7):2108–2119, 2013.

67. Yi Ling Chen and Michael Habeck. Data-driven coarse graining of large biomolecular structures. *PLoS ONE*, 12(8):1–17, 2017.

68. C. Scherer and D. Andrienko. Comparison of systematic coarse-graining strategies for soluble conjugated polymers. *European Physical Journal: Special Topics*, 225(8-9):1441–1461, 2016.

69. Karteek K. Bejagam, Samrendra Singh, Yaxin An, and Sanket A. Deshmukh. Machine-Learned Coarse-Grained Models. *The Journal of Physical Chemistry Letters*, 9(16):4667–4672, 2018.

70. Victor Ruhle, Christoph Junghans, Alexander Lukyanov, Kurt Kremer, and Denis Andrienko. Versatile Object-Oriented Toolkit for Coarse-Graining Applications. *Journal of Chemical Theory and Computation*, 5(12):3211–3223, 2009.

71. Christoph Scherer and Denis Andrienko. Understanding three-body contributions to coarse-grained force fields. *Physical Chemistry Chemical Physics*, 20(34):22387–22394, 2018.

72. Lanyuan Lu, James F. Dama, and Gregory A. Voth. Fitting coarse-grained distribution functions through an iterative force-matching method. *Journal of Chemical Physics*, 139(12), 2013.

73. Dilnoza B Amirkulova and Andrew D White. Combining Enhanced Sampling with Experiment Directed Simulation of the GYG peptide. *J. Theor. Comput. Chem.*, 17(3):1840007, 2018.

74. Andrew D White and Gregory A Voth. Efficient and Minimal Method to Bias Molecular Simulations with Experimental Data. *J. Chem. Theory Comput.*, 2014.

75. Andrew D. White, James F. Dama, and Gregory A. Voth. Designing Free Energy Surfaces That Match Experimental Data with Metadynamics. *Journal of Chemical Theory and Computation*, 11(6):2451–2460, 2015.

76. Andrew D. White, Chris Knight, Glen M. Hocky, and Gregory A. Voth. Communication: Improved ab initio molecular dynamics by minimally biasing with experimental data. *J. Chem. Phys.*, 146(4):041102, 2017.

77. Thomas Dannenhoffer-Lafage, Andrew D. White, and Gregory A. Voth. A Direct Method for Incorporating Experimental Data into Multiscale Coarse-Grained Models. *J. Chem. Theory Comput.*, 12(5):2144–2153, 2016.

78. Dilnoza B Amirkulova and Andrew D White. Recent Advances in Maximum Entropy Biasing Techniques for Molecular Dynamics. *Submitted*, feb 2019. https://arxiv.org/abs/1902.02252.

79. Benjamin Chu and Tianbo Liu. Characterization of nanoparticles by scattering techniques. *Journal of Nanoparticle Research*, 2(1):29–41, Mar 2000.

80. Stewart F Parker and Paul Collier. Applications of Neutron Scattering in Catalysis Where atoms are and how they move Neutron Properties and their Applications. *Johnson Matthey Technol. Rev*, 60(2):132–144, 2016.

81. Felix Fernandez-Alonso and David L. (David Long) Price, editors. *Neutron scattering : applications in biology, chemistry, and materials science.* Academic Press, 2017.

82. Sven Vogel. A review of neutron scattering applications to nuclear materials. *ISRN Mat. Sci.*, 2013, 08 2013.

83. Jeremy C Smith, Pan Tan, Loukas Petridis, and Liang Hong. Dynamic Neutron Scattering by Biological Systems. *Annual Review of Biophysics*, 47:335 – 354, 2018.

84. Christopher L. Farrow and Simon J. L. Billinge. Relationship between the atomic pair distribution function and small-angle scattering: implications for modeling of nanoparticles. *Acta Crystallographica Section A*, 65(3):232–239, May 2009.

85. Varley F Sears. Special Feature Neutron scattering lengths and cross sectioirn. *Neutron News*, 3(3):26–37, 1992.

86. Katrin Amann-Winkel, Marie-Claire Bellissent-Funel, Livia E. Bove, Thomas Loerting, Anders Nilsson, Alessandro Paciaroni, Daniel Schlesinger, and Lawrie Skinner. X-ray and neutron scattering of water. *Chemical Reviews*, 116(13):7570–7589, 2016. PMID: 27195477.